Biosensors and Bioelectronics 130 (2019) 65–72

Contents lists available at ScienceDirect

Biosensors and Bioelectronics

journal homepage: www.elsevier.com/locate/bios

Nanoscale fluorescent metal–organic framework composites as a logic platform for potential diagnosis of asthma

Xin Zhang, Liquan Fang, Ke Jiang, Huajun He, Yu Yang, Yuanjing Cui, Bin Li*, Guodong Qian*

State Key Laboratory of Silicon Materials, Cyrus Tang Center for Sensor Materials and Applications, School of Materials Science and Engineering, Zhejiang University, Hangzhou 310027, China

ARTICLE INFO

Keywords:
Asthma
Metal–organic frameworks
Chemical sensing
Logic gate
Hydrogen sulfide

ABSTRACT

Asthma is a common chronic disorder, and the decreased hydrogen sulfide (H_2S) production in the lung has been considered as an early detection biomarker for asthma. However, the detection of H_2S in biological systems remains a challenge; because it requires the designed sensors to have the following features: nanoscale size, good biocompatibility, real-time detection, high selectivity/sensitivity, and good water stability. Here, we propose the potential of using nanoscale fluorescent metal–organic framework (MOF) composites Eu^{3+}/Ag^{+}@UiO-66-$(COOH)_2$ (hereafter denoted as **EAUC**) as a logic platform for tentative diagnosis of asthma by detecting the biomarker H_2S. This INHIBIT logic gate based on Eu^{3+}@UiO-66-$(COOH)_2$ (**EUC**) can be produced by choosing Ag^{+} and H_2S as inputs and by monitoring the fluorescent signal (I_{615}) as an output. Our fluorescent studies indicate that the **EAUC** exhibits excellent selectivity, extreme sensitivity (limit of detection: 23.53 μM), and real-time in situ detection of H_2S. Further, MTT analysis in PC12 cells shows that the **EAUC** possesses low cytotoxicity and favourable biocompatibility that are suitable for the detection of biomarker H_2S in vivo, as demonstrated by the successful detection of spiked H_2S in the diluted serum samples. This work represents the possibility of using MOF-based logic platform for tentative diagnosis of asthma in clinical medicine.

1. Introduction

Asthma is a complex chronic inflammatory disease of the airways that involves the activation of many inflammatory and structural cells (Barnes, 1996). Recent biological studies have indicated that hydrogen sulfide (H_2S) is associated with various physiological and pathological processes (Kimura, 2011; Szabó, 2007; Wen et al., 2013); for example, H_2S can be produced in the lung and airway tissues via the actions of two H_2S-generating enzymes, cystathionine β-synthase (CBS) and/or cystathionine γ-lyase (CSE). And serum H_2S levels would be significantly reduced in asthma patients, considered as an early detection biomarker for asthma (Wang et al., 2011). Various methods towards H_2S detection, including colorimetric/electrochemical assays, gas chromatography, and sulfide precipitations, are available to measure H_2S in blood plasma and homogenized tissues; however, they often require complicated post-mortem processing and/or destruction of tissues or cell lysates (Doeller et al., 2005; Tangerman, 2009; Ubuka, 2002). In this regard, the fluorescence-based detecting methods are preferred due to their high sensitivity, simplicity, short response time, non-invasive nature, and real-time monitoring (Chen et al., 2013; Liu et al., 2011).

A large number of fluorescent materials have been developed for the detection of H_2S in aqueous solution or biological systems (Cao et al., 2017; Dalapati et al., 2017). Their practical applications are commonly hampered by the complicated fluorescence signals that are hard to identify for the public. Therefore, the sensing materials should be deviceized in order to transfer the complicated fluorescence signals to the easily identifiable electronic signals, especially for biometric recognition and diagnosis (Madhuprasad et al., 2016; Stassen et al., 2017). Molecular logic gates are the fundamental components of electronic and digital circuit that have shown great potential for applications in the field of life sciences (Guo et al., 2010; Hettie et al., 2014; Zhang et al., 2012). It is of great importance to construct a practical logic device which can recognize the certain analytes with high selectivity/sensitivity in one system (Bozdemir et al., 2010; Wu et al., 2013; Yuan et al., 2008). In this regard, the emerging metal–organic frameworks (MOFs), built from metal ions and organic linkers (Jiang et al., 2018; Li et al., 2016, 2018; Wen et al., 2018), have been explosively developed as a kind of promising materials for various chemical sensors (Cui et al., 2015; Wales et al., 2015). In recent years, several fluorescent MOF materials have been reported to be a logic platform for environmental or food spoilage monitoring. Despite a significant progress, the

* Corresponding authors.
E-mail addresses: bin.li@zju.edu.cn (B. Li), gdqian@zju.edu.cn (G. Qian).

https://doi.org/10.1016/j.bios.2019.01.011
Received 21 October 2018; Received in revised form 27 December 2018; Accepted 3 January 2019
Available online 15 January 2019
0956-5663/

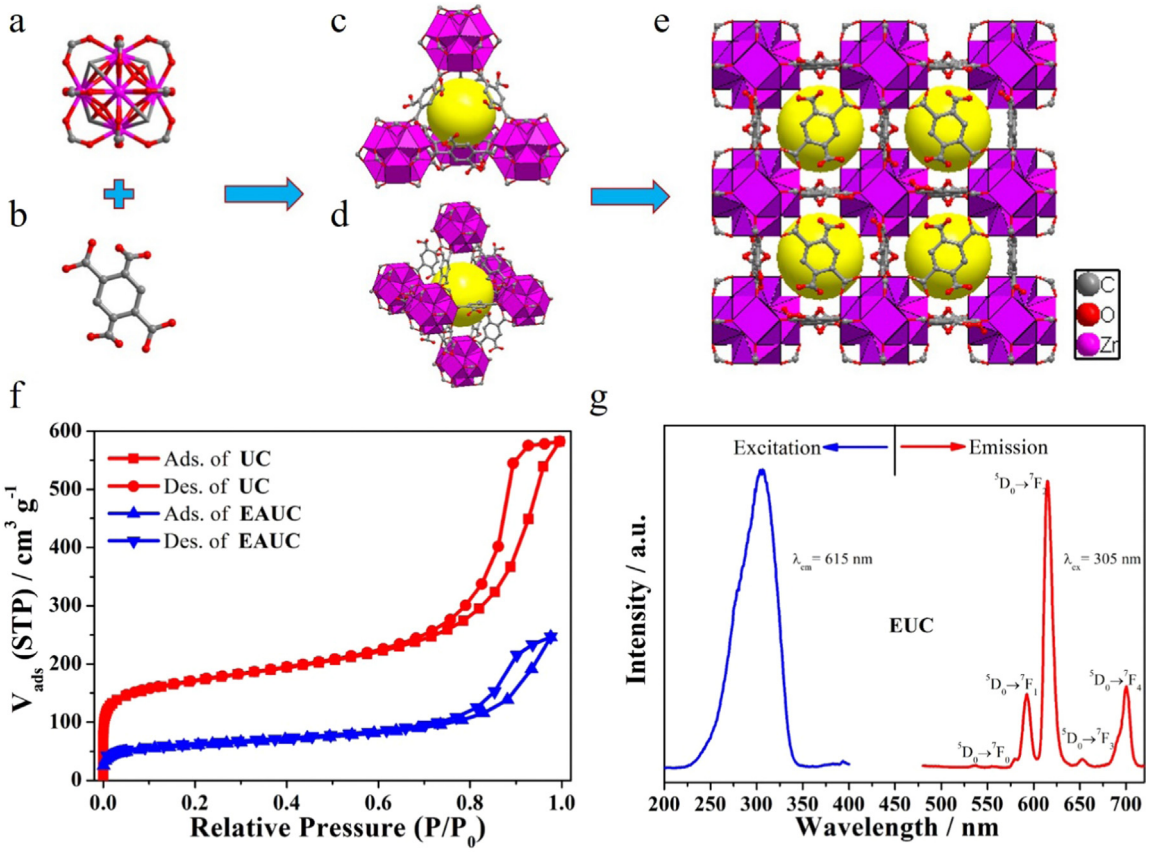

Fig. 1. (a) Ball and stick representation of SBU (gray: C; red: O; pink: Zr). (b) The H_4btec ligand. (c) The tetrahedral cage. (d) The octahedral cage. (e) The **UC** structure. (f) N_2 adsorption-desorption isotherms of **UC** (red) and **EAUC** (blue) at 77 K. (g) Emission spectrum and excitation spectrum of **EUC** (λ_{ex} = 305 nm, λ_{em} = 615 nm). The yellow spheres represent the void regions.

potential of using MOF-based sensors to construct logic gates for detection of asthma biomarker H_2S in biological samples has not been established yet. For biological sensing applications, the designed sensor or logic platform should have nanoscale size, good biocompatibility, real-time detection, high selectivity/sensitivity, and good water stability (Li et al., 2016; Lu et al., 2018).

In this work, we herein developed and established a fluorescent MOF-based logic platform Eu^{3+}/Ag^{+}@UiO-66-$(COOH)_2$ (**EAUC**), and realized its potential for detection of asthma biomarker H_2S in biological samples for the first time. The key point of this platform is to introduce the active metal centers (Ag^{+}) to the Eu^{3+}@UiO-66-$(COOH)_2$ (**EUC**, Figs. 1 and 2 a) as the lanthanide-luminescence sensitizer and H_2S-responding site (Chen et al., 2010; Ma et al., 2013; Nonat et al., 2009). As a result, the INHIBIT logic gate based on **EUC** can use Ag^{+} and H_2S as two inputs and the fluorescence intensity of **EUC** as the output signal. This MOF-based probe exhibits rapid response, excellent selectivity, and extreme sensitivity in situ detection of H_2S over other environmentally and biologically relevant species under physiological conditions. In particular, the MTT assay and cell viability studies in PC12 cells indicated that the **EAUC** has relatively low cytotoxicity and excellent biocompatibility that are suitable for the detection of biomarker H_2S in vivo. Most importantly, the detection of H_2S by the **EAUC** platform has been achieved in the diluted serum samples with spiked H_2S. These results demonstrated the possibility of using MOF-based logic platform for detecting H_2S in biological samples, offering a potential method for conveniently tentative diagnosis of asthma.

2. Experimental section

2.1. Synthesis of UiO-66-$(COOH)_2$

The UiO-66-$(COOH)_2$ (hereafter denoted as **UC**) solid was synthesized based on the previously reported procedure with slight modification (Yang et al., 2013).

2.2. Preparation of EUC and EAUC

EUC was prepared by heating the mixture of 0.1 g compound **UC** and 0.446 g (1 mmol) $Eu(NO_3)_3{\cdot}6H_2O$ in 10 mL distilled water at 60 °C for 24 h. **EAUC** was prepared by heating the mixtures of 0.1 g compound **UC**, 0.446 g (1 mmol) $Eu(NO_3)_3{\cdot}6H_2O$ and 0.170 g (1 mmol) $AgNO_3$ in 10 mL distilled water at 60 °C for 24 h. The solid was isolated by centrifugation for 10 min at 8000 rpm, washed with distilled water followed by exchanging it with acetone over 5 days. During this period, acetone was freshly exchanged 3 times per day. Then, the volatile acetone was removed under vacuum at 70 °C.

2.3. Real sample analysis

The standard addition technique was used for the determination of H_2S in the diluted fetal bovine and human serum samples. Considering the autofluorescence of serum, 100-fold diluted serum was selected for the test to avoid the possible interference. A sample volume of 50 μL of the serum sample was diluted to 5 mL with 10 mM HEPES buffer (pH 7.4). Then, different concentration of H_2S was added to the 100-fold diluted serum samples.

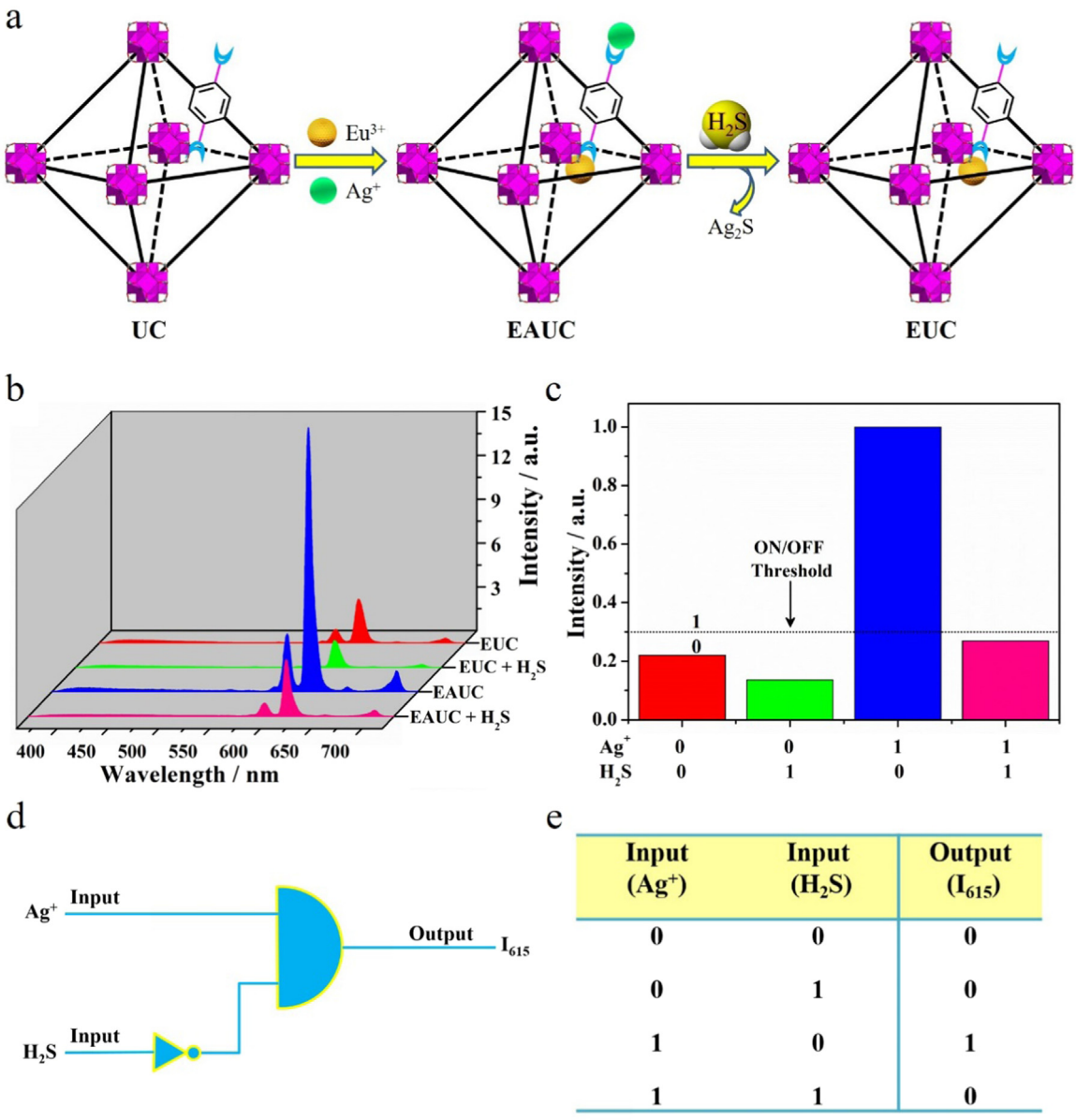

Input (Ag^+)	Input (H_2S)	Output (I_{615})
0	0	0
0	1	0
1	0	1
1	1	0

Fig. 2. (a) Synthetic scheme and representative crystalline structure: the tetrahedral cage of **UC**, **EAUC**, and **EUC**. (b) Fluorescence spectra of **EUC** in the presence of four input modes: (red) no input; (green) 5 mM H_2S; (blue) 1 mM Ag^+; (pink) 5 mM H_2S + 1 mM Ag^+. (c) Fluorescence intensity changes at 615 nm in the form of a bar representation, with a threshold of I_{615} = 0.3 (normalized fluorescence intensity) for output 1 or 0. (d) INHIBIT logic gate represented using a conventional gate notation. (e) Truth table for the INHIBIT logic gate; Ag^+ and H_2S are inputs to the system; fluorescence intensity I_{615} is the output signal of **EUC**.

3. Results and discussion

3.1. Design and characterization of EUC and EAUC

As a UiO-66 analogue, UiO-66-$(COOH)_2$ (hereafter denoted as **UC**) was selected as a parent framework due to its exceptionally chemical and thermal stability (Luan et al., 2015; Yang et al., 2011a, 2011b). **UC** consists of Zr_6-octahedra $[Zr_6O_4(OH)_4]$ secondary building units (SBUs), bridged by benzene-1,2,4,5-tetracarboxylic acid (H_4btec) ligand to form a three-dimensional (3D) microporous structure with octahedral and tetrahedral cages (D. Wu et al., 2014) (Fig. 1). The powder X-ray diffraction (PXRD) patterns demonstrated that **UC** is isostructural to UiO-66 (Fig. S1). Scanning electron microscopy (SEM) and transmission electron microscopy (TEM) images showed that the sizes of **UC** particles are 80–100 nm (Fig. S2). Small particle size is beneficial to the dispersion of **UC** in the solution. We note that only two carboxylate arms of the H_4btec act as linkers in the **UC**, while the rest of two carboxylates are uncoordinated and keep their protonated form of –COOH. The free –COOH group was evidenced by FT-IR spectrum with a typical peak at 1716 cm^{-1}, attributed to the C=O stretching vibration of the –COOH (Fig. S3). The N_2 adsorption isotherm of **UC** shows a highly porous material with Brunauer-Emmett-Teller (BET) surface area of 620 m^2g^{-1}, lower than that of UiO-66 (1110 m^2g^{-1}) due to the uncoordinated -COOH groups (Garibay and Cohen, 2010) (Fig. 1f). The reactive nature of uncoordinated -COOH combined with the permanent porosity of **UC** render it as a good candidate to bind with metal cations (Biswas and Van Der Voort, 2013). ICP-MS analysis, FT-IR spectra, PXRD patterns, and photoluminescence properties have been implemented to verify the successful binding of Eu^{3+} with the free -COOH. Firstly, the Eu^{3+} loading content in **EUC** was determined by inductively coupled plasma-mass spectrometry (ICP-MS). The molar ratio of Zr:Eu was calculated to be 2.28:1 (Table S1). In addition, the FT-IR absorption of -COOH at 1716 cm^{-1} in **EUC** was found to be much weaker than that in **UC**, further proving the successful binding of Eu^{3+}

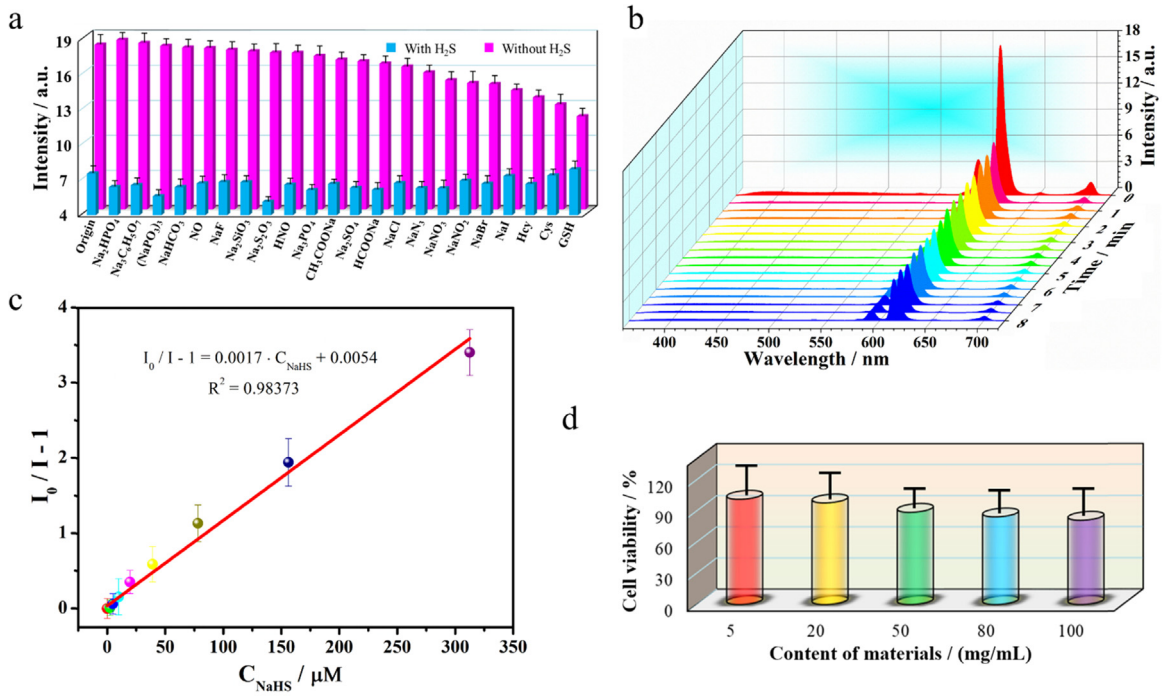

Fig. 3. (a) Fluorescence responses of **EAUC** upon addition of other various analytes (pink) followed by addition of H_2S (wathet). (b) Fluorescence intensity of **EAUC** at 615 nm towards addition of H_2S (5 mM) after 0–8 min (c) Concentration (0–312.5 μM) dependence of the fluorescence intensity (I_{615}). (d) MTT assay of **EAUC** obtained from incubation with PC12 cells.

with the free -COOH (Fig. S3). The incorporation of Eu^{3+} induced no change in the structure and crystalline integrity (Fig. S1). The successful constitution of **EUC** was also verified by the spectra in HEPES buffer (pH 7.4). The emission spectrum of **EUC** excited at 305 nm indicates well-resolved magnified luminescence of the f-f transitions, assigned to the energy transfer from H_4btec ligands to Eu^{3+} ions. Characteristic emissions of the Eu^{3+} ions are also obvious with peaks at 579, 592, 615, 651, and 700 nm (Fig. 1g), arising from its $^5D_0$ excited state to $^7F_0$, $^7F_1$, $^7F_2$, $^7F_3$, and $^7F_4$ ground state, respectively.

A new class of lanthanide luminescent MOFs was generated by encapsulating Eu^{3+} into **UC** crystals (Hao and Yan, 2015). The key point of the probe design is to introduce the reactive sites of H_2S into the framework. Considering the easy functionalization of MOFs, the design could be achieved by introducting active metal centers (Ag^+) into the framework as H_2S- reactive sites. Additionally, Ag^+ ions in aqueous solution have been found to be able to sensitize the fluorescence of Eu^{3+} ions (Hao and Yan, 2014; Xiao et al., 2010). Compared with the previously reported Eu^{3+}/Cu^{2+}@UiO-66-$(COOH)_2$ (Zhang et al., 2016), the design of **EAUC** has the following two reasons: i) **EAUC** has much stronger lanthanide luminescence than Eu^{3+}/Cu^{2+}@UiO-66-$(COOH)_2$ due to the sensitization of Ag^+ ions, which can significantly enhance the signal-to-noise ratio and thus improve the accuracy of detection (Fig. S4); ii) respiratory virus infection is a major cause of asthma attacks, and Ag^+ ions are an important antibacterial agent (Marambio-Jones and Hoek, 2010; Rai et al., 2009). These factors inspired us to incorporate Ag^+ ions into **EUC** to form a luminescence-enhanced **EAUC** (Fig. 2a). The ICP-MS analysis, N_2 sorption isotherm, FT-IR spectra, PXRD patterns, and photoluminescence properties have been performed to verify the success of introducing Ag^+ into **EUC**. The ICP-MS measurement indicated that the Zr:Eu:Ag molar ratio is 6.83:2.91:1 in **EAUC** (Table S1). As shown in Fig. S3, the band of uncoordinated -COOH groups at 1716 cm^{-1} almost disappeared, illustrating the coordination interactions between metal cations (Eu^{3+} and Ag^+) and uncoordinated -COOH. The BET surface area of **EAUC** is ~197 m^2g^{-1}, showing a reasonable derease compared with **EUC** (620 m^2g^{-1}) due to the encapsulation of Ag^+ ions (Fig. 1f). The Eu^{3+} and Ag^+ loaded samples can maintain the integrity of the framework, as confirmed by the PXRD (Fig. S1). After the incorporation of Ag^+, the fluorescence intensity of Eu^{3+} in **EAUC** is much higher than that of **EUC** (Fig. 2b and c). This further verifies that Ag^+ ions have been successfully encapsulated into **EAUC** for sensitizing the Eu^{3+} luminescence.

3.2. Construction of an INHIBIT logic platform

The inclusion of Ag^+ ions can lead to a more efficient energy transition from H_4btec ligands to Eu^{3+} for the following grounds: (1) a variety of non-radiative deactivations and energy loss can be reduced when Ag^+ is successfully encapsulated inside the framework (Tan and Chen, 2011); (2) the heavy atom effect of Ag^+ ions can facilitate the intersystem crossing energy transfer ($S_1 \rightarrow T_1$) (Barbieri et al., 2008; Liu et al., 2012); (3) the d^{10} closed shell electronic configuration of Ag^+ allows the d-d transition. Due to the charge transfer of H_4btec ligands to Eu^{3+}, the energy level of the excited state of H_4btec ligands can be modified, making the energy-matching more appropriate between H_4btec ligands and Eu^{3+} ions (Cui et al., 2012; Ma et al., 2013). All these reasons result in a more effective intramolecular energy transfer from H_4btec ligands to Eu^{3+}, thus benefiting the Eu emission. However, in the presence of H_2S, the fluorescence of **EAUC** can be quenched strongly (Fig. 2b and c). This is because sulfide has a strong affinity toward Ag^+ ions, which can destroy the sensitization of Ag^+ ions. After addition of H_2S into **EAUC**, the material retained its crystallinity well, as evidenced by the PXRD pattern (Fig. S5).

From the above fluorescence studies, we believe that **EUC** can serve as an INHIBIT logic gate since the intensity of the emission at 615 nm is responsive to the presence or absence of Ag^+ and H_2S. Thus, the logic gate properties of **EUC** can be established by using two input signals of Ag^+ (Input1) and H_2S (Input2), respectively. The presence and absence of two inputs Ag^+ and H_2S can be defined as "1" and "0" states. Monitoring the fluorescent emission of **EUC** at 615 nm as the output. The output value below the predefined threshold level (0.3, normalized fluorescence intensity) is translated into binary "0", while the fluorescence output value above the threshold corresponds to binary "1". As

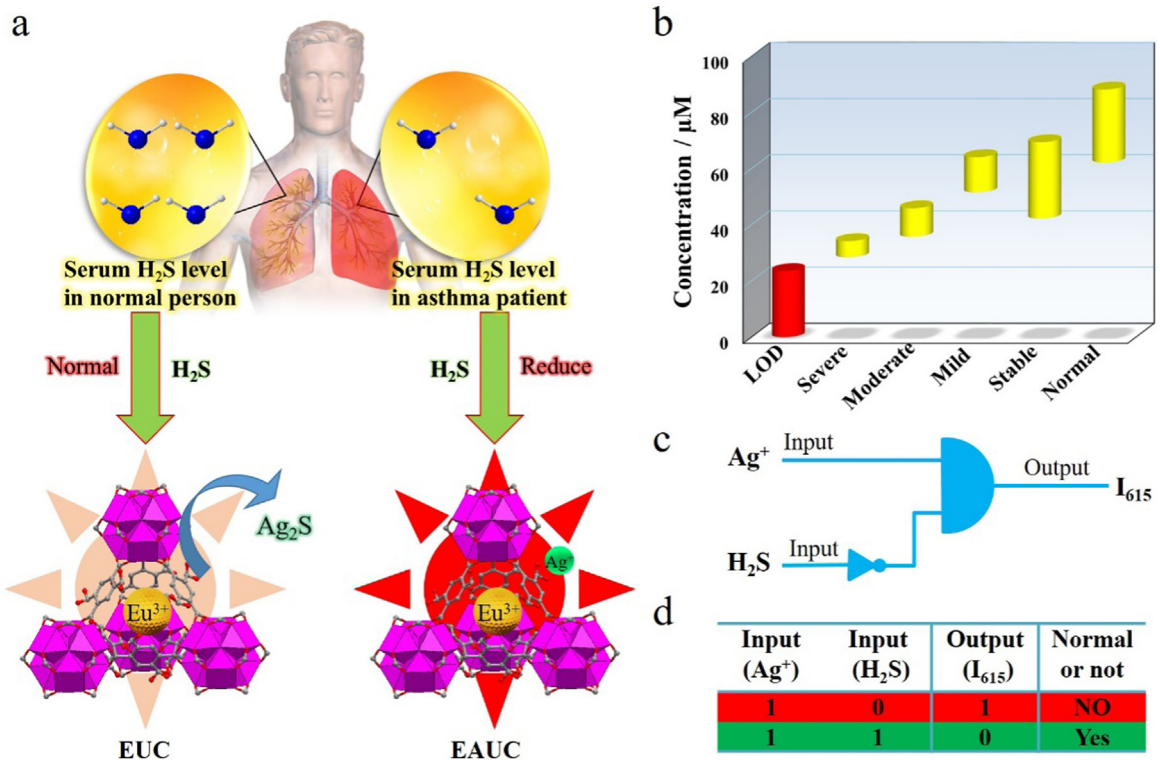

Fig. 4. (a) The principle of the initial diagnosis of asthma. (b) The relationship between asthma and the concentration of H_2S. (c) INHIBIT logic gate represented using a conventional gate notation; an active output signal is obtained when Ag^+ = 1 and H_2S = 0. (d) Truth table for the INHIBIT logic gate.

shown in Fig. 2b and c, the fluorescence intensity I_{615} (Output) of the **EUC** is distinctly high (output = 1) only when (Input1, Input2) is (1, 0). In contrast, the fluorescence intensity I_{615} holds a low level (output = 0) when (Input1, Input2) is (0, 0), (0, 1), or (1, 1), respecitvely. The pictorial representation and the truth table for the corresponding INHIBIT are given in Fig. 2d and e.

3.3. Sensing properties of EAUC

High selectivity is quite significant and important to target an excellent chemosensor. To verify whether other anions and amino acids have such a quenching behavior with H_2S, we tested the effect of F^-, Cl^-, Br^-, I^-, $HCOO^-$, CH_3COO^-, NO_2^-, NO_3^-, HPO_4^{2-}, PO_4^{3-}, $P_3O_9^{3-}$, $S_2O_3^{2-}$, SO_4^{2-}, HCO_3^-, N_3^-, SiO_3^{2-}, $C_6H_5O_7^{3-}$, L-Leucine (Leu), L-Cysteine (Cys), and glutathione (GSH) on the fluorescence intensity of **EAUC**. As shown in Fig. 3a, only the addition of H_2S can generate remarkable fluorescence quenching, while very weak variations were observed upon addition of other analytes in the same conditions. Cys and GSH can slightly reduce the fluorescence of **EAUC**, possibly attributed to the coordination of the thiol group with Ag^+ ions that can weaken the sensitization of Ag^+ to Eu^{3+}. These results illustrate that these anions and thiol-containing Cys and GSH have a negligible impact on the detection of H_2S. In accordance with Pearson's hard-soft acid-base theory (Pearson, 1963), Ag^+ is a soft ion (soft acid) which can preferentially interact with sulfide (a soft base). The high selectivity of **EAUC** toward H_2S might be attributed to the ultrastrong binding ability of Ag^+ ion with sulfide, where the solubility product constant of Ag_2S (K_{sp} = 6.3×10^{-50}) is approximately at least 30 orders of magnitude lower than that of Ag^+ with other anions (Liu and Chen, 2013).

For real-time applications, selective and efficient detection is critical in the presence of potentially interfering environmentally and biologically important analytes. The solution containing **EAUC** and H_2S in HEPES buffer (pH 7.4) was first treated with competing analyte, and the fluorescence response was recorded (Fig. 3a). H_2S displayed a remarkable fluorescence quenching effect even in the presence of competing analytes. This indicates that the selective detection of H_2S by **EAUC** can be fulfilled in complex biological systems without off-target reactivity and false response.

The response time is another important factor of fluorescence sensors, particularly in organisms with a fast metabolism. We thus investigated the time course of the precipitation reaction of the **EAUC** sensor towards H_2S. As demonstrated in Fig. 3b and S6, the sulfide-induced fluorescence quenching response is extremely rapid. The emission intensity of Eu^{3+} at 615 nm has been declined sharply within 30 s, and then it began to decrease slowly. Considering the variable and rapid metabolism nature of endogenous H_2S in biological systems, this rapid response reveals the potential of **EAUC** in real-time intracellular H_2S imaging.

We monitored the fluorescence response of **EAUC** under various concentrations of H_2S. As shown in Fig. S7 and S8, the good relationship (correlation coefficient R^2 = 0.9945) betwwen its fluorescence intensity and H_2S concentration in the range of 0–2.5 mM can be set up as a function of $I_0/I = -0.85 \cdot \exp(-0.003 \cdot C_{H_2S}) + 1.85$. This signifies that **EAUC** can be used for the quantitative detection of H_2S. As depicted in Fig. 3c, when the H_2S concentration increased from 0 to 312.5 μM, the emission intensity of **EAUC** was quenched by degrees. A good linear relationship (R^2 = 0.98373) between the emission intensity of Eu^{3+} at 615 nm and the concentration of H_2S was observed. The fluorescence intensity *vs* C_{H_2S} plot can be curve-fitted into $I_0/I - 1 = 0.0017 \cdot C_{H_2S} + 0.0054$, close to the Stern-Volmer equation (Thomas et al., 2007): $I_0/I - 1 = K_{SV} C_{H_2S}$ where I_0 and I are the luminescent intensity before and after H_2S incorporation, respectively; K_{SV} is the Stern-Volmer constant; and C_{H_2S} is the H_2S molar concentration. On the basis of the experimental data in Fig. 3c, the K_{SV} value was calculated to be 1.7×10^3 M^{-1}, illustrating a strong quenching effect on the luminescence of **EAUC** (Nagarkar et al., 2014; Zheng et al., 2013; Zhou et al., 2014). As shown in Fig. 3c, the limit of detection (LOD) value of **EAUC** towards H_2S was calculated to be 23.53 μM. Compared with other existing materials for detecting H_2S, **EAUC** has a faster response time and the detection sensitivity is comparable to the best-performing materials

(Mao et al., 2013; Qian et al., 2011; Yu et al., 2012) (Table S2). Previous studies have already showed that the serum level of H_2S decreases from 75.2 ± 13.0 μM in healthy subjects to 55.8 ± 13.6 μM in patients with stable asthma, 57.8 ± 6.3 μM in patients with mild of acute exacerbation asthma, 40.8 ± 5.1 μM in patients with moderate of acute exacerbation asthma, and 31.3 ± 2.9 μM in patients with severe acute exacerbation of asthma (Wu et al., 2008) (Fig. 4). On the basis of the above data, the LOD of **EAUC** is low enough to meet the preliminary diagnosis of asthma. The content of H_2S can be calculated by the fluorescence intensity output of the logic platform to determine whether it is suffering from asthma. This luminescent INHIBIT logic platform thus offers a new opportunity for tentative diagnosis of asthma disease associated with H_2S detection in clinical medicine (Fig. 4).

3.4. Biocompatibility and cytotoxicity of EAUC

The foregoing results indicate that **EAUC** holds a great potential as a fluorescent sensor for detection of asthma biomarker. For the use in biologic applications, the biocompatibility and cytotoxicity of **EAUC** need to be further evaluated to verify its significance. As depicted in Fig. 3d, we found that the cell viability decreased slightly with the **EAUC** concentration increased. The cell viability is still above 80% even if the concentration of **EAUC** reached up to 100 μg/mL, indicating that **EAUC** shows negligible cytotoxicity as a candidate for H_2S sensing in biological fluids.

Optical microscopy graphs were utilized to validate the potential of **EAUC** towards monitoring H_2S chemistry in vivo. PC12 cells were cultured with different concentrations (0, 10, and 20 μg mL^{-1}) of **EAUC** for 24 h. Their morphology was analyzed by optical microscopy. No severe distinction can be observed in the morphology of PC12 cells between the MOF-incubated cells and the control cells (Fig. 5). A large number of MOF particles were observed and segregated in the cytosol by the endocytosis, as shown in Fig. 5b. After the incubation with **EAUC**, the appreciable neuritis extension of PC12 cells convincingly indicated the good biocompatibility and negligible cytotoxicity of **EAUC**. As shown in Fig. 5, PC12 cells loaded with 20 mg mL^{-1} of **EAUC** show extremely strong red emission with an excitation of 315 nm. A significant attenuation of fluorescence intensity was observed after incubating the 10^{-4} M NaHS solution into the cells within 5 min. It is suggested that probe **EAUC** is suitable for the application in fluorescent H_2S sensing in living cells.

3.5. Real sample analysis

To examine the applicability of **EAUC** in real biological samples, the determination of H_2S was performed in the diluted fetal bovine and human serum samples (Liu et al., 2013; Pak et al., 2016; P. Wu et al., 2014). Considering the strong autofluorescence of serum (Soini and Hemmilä, 1979; Wang et al., 2017), 100-fold diluted serum was selected for sample treatment to avoid the possible interference caused by the biomolecules in serum (Qian et al., 2014; Wang et al., 2018; Yang et al., 2014). The luminescence intensity and PXRD of **EAUC** showed that no obvious change was found in the diluted serum samples (Figs. S9 and S10), confirming its good stability in serum samples. A standard addition method was used to detect the level of H_2S in the diluted serum samples (Table 1). The recoveries for the H_2S measurement in three spiked samples range from 97.3% to 102.8%, with RSD (n = 3) values less than 3.8%. Moreover, we also detected H_2S in 10-fold diluted human serum samples (Table S3). We found that this sensing material can also work in this serum sample; however, the recoveries

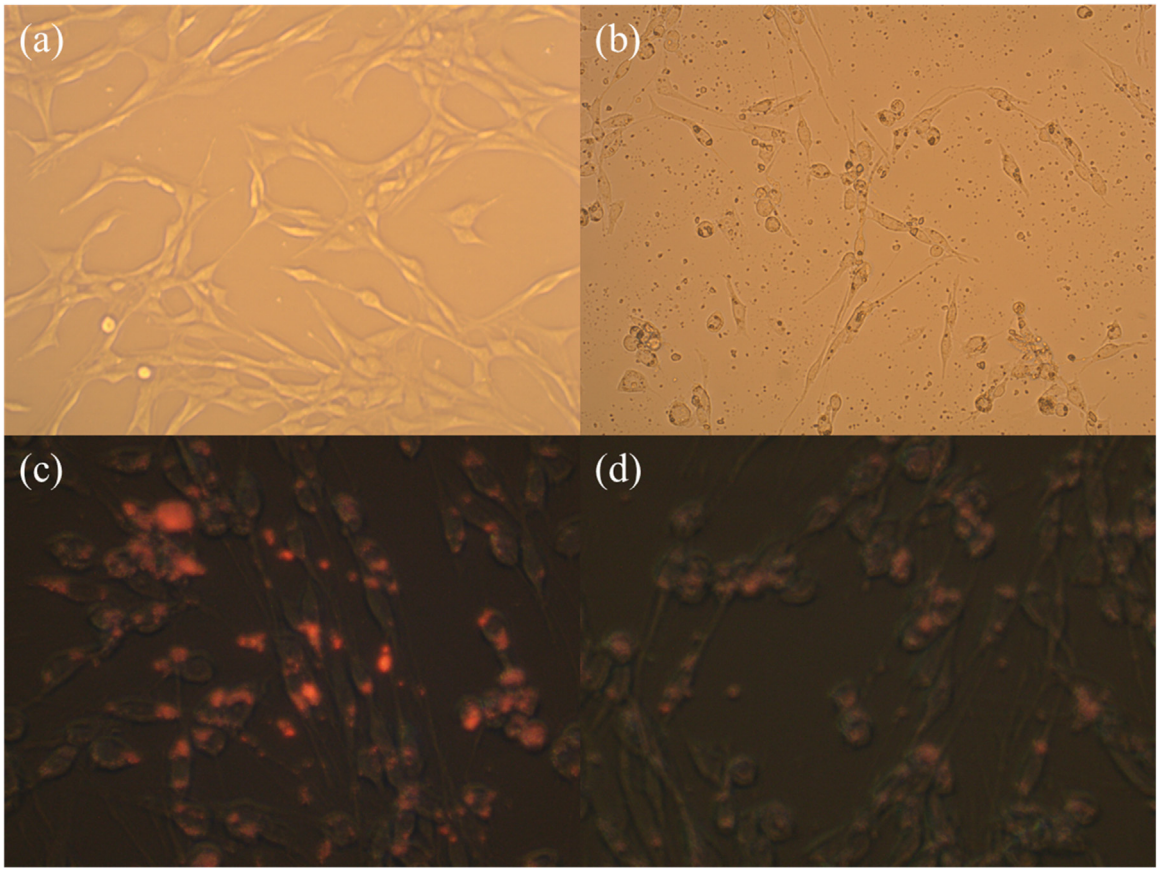

Fig. 5. Optical microscopy images of PC12 cells without **EAUC** (a) and PC12 cells incubated with **EAUC** of 10 μg mL^{-1} for 24 h (b). Fluorescent images of PC12 cells incubated with 20 μg mL^{-1} **EAUC** for 24 h (c). Fluorescent images of PC12 cells incubated with 20 μg mL^{-1} **EAUC** for 24 h, followed by incubation with 10^{-4} M NaHS for 5 min (d). The wavelength for excitation is 315 nm.

Table 1
Determination of H_2S in the diluted serum samples using **EAUC**.

	Sample	Added (μM)	Found (μM)	Recovery (%)	RSD (%)
Fetal bovine serum	Sample 1	40	40.6	101.5	2.1
	Sample 2	60	58.4	97.3	2.8
	Sample 3	80	81.7	102.1	1.6
Human serum	Sample 1	40	39.1	97.8	3.8
	Sample 2	60	59.4	99.0	3.2
	Sample 3	80	82.2	102.8	2.6

and RSD are relatively higher than that observed in 100-fold serum due to the matrix effects. All of the characteristic parameters for the method validated that this sensing platform can be used to detect H_2S in real biological samples.

4. Conclusions

In summary, we have realized the potential of using fluorescent MOF composites **EAUC** for tentative diagnosis of asthma by detecting the biomarker H_2S in biological systems. The foregoing fluorescent studies indicated that the **EAUC** sensor exhibits rapid response, excellent selectivity, and high sensitivity toward in situ detection of H_2S, comparable to the best-performing materials reported. An INHIBIT logic gate was further established based on the **EAUC** by choosing Ag^+ and H_2S as the inputs and the intensity of fluorescent signal (I_{615}) as the output. Combined with its nanoscale size, excellent biocompatibility and low cytotoxicity, the **EAUC** logic platform has been successfully used for H_2S detection in both PC12 cells and the diluted serum samples, demonstrating its sensing feasibility in vivo. This work might open a new method to develop MOF-based logic platform for noninvasively tentative diagnosis of diseases.

CRediT authorship contribution statement

Xin Zhang: Data curation, Formal analysis, Investigation, Methodology, Writing - original draft. **Liquan Fang:** Data curation, Writing - original draft. **Ke Jiang:** Data curation, Formal analysis. **Huajun He:** Formal analysis. **Yu Yang:** Methodology. **Yuanjing Cui:** Formal analysis, Methodology, Resources. **Bin Li:** Conceptualization, Funding acquisition, Investigation, Project administration, Resources, Supervision, Writing - review & editing. **Guodong Qian:** Conceptualization, Funding acquisition, Investigation, Project administration, Resources, Supervision, Writing - review & editing.

Acknowledgements

The authors gratefully acknowledge the financial support for this work from the National Natural Science Foundation of China (Nos. 61721005, 51472217, 51432001, 51632008, and U1609219), Natural Science Foundation of Zhejiang Province of China (No. LZ15E020001) and the Fundamental Research Funds for the Central Universities (2018QNA4010).

Appendix A. Supporting information

Supplementary data associated with this article can be found in the online version at doi:10.1016/j.bios.2019.01.011.

References

Barbieri, A., Accorsi, G., Armaroli, N., 2008. Chem. Commun. 19, 2185–2193.
Barnes, P.J., 1996. Br. J. Clin. Pharmacol. 42 (1), 3–10.
Biswas, S., Van Der Voort, P., 2013. Eur. J. Inorg. Chem. 12, 2154–2160.
Bozdemir, O.A., Guliyev, R., Buyukcakir, O., Selcuk, S., Kolemen, S., Gulseren, G., Nalbantoglu, T., Boyaci, H., Akkaya, E.U., 2010. J. Am. Chem. Soc. 132 (23), 8029–8036.
Cao, Y.-Y., Guo, X.-F., Wang, H., 2017. Sens. Actuators B: Chem. 243, 8–13.
Chen, F.F., Chen, Z.Q., Bian, Z.Q., Huang, C.H., 2010. Coord. Chem. Rev. 254 (9), 991–1010.
Chen, Y., Zhu, C., Yang, Z., Chen, J., He, Y., Jiao, Y., He, W., Qiu, L., Cen, J., Guo, Z., 2013. Angew. Chem. Int. Ed. 52 (6), 1688–1691.
Cui, Y., Song, R., Yu, J., Liu, M., Wang, Z., Wu, C., Yang, Y., Wang, Z., Chen, B., Qian, G., 2015. Adv. Mater. 27 (8), 1420–1425.
Cui, Y., Yue, Y., Qian, G., Chen, B., 2012. Chem. Rev. 112 (2), 1126–1162.
Dalapati, R., Balaji, S.N., Trivedi, V., Khamari, L., Biswas, S., 2017. Sens. Actuators B: Chem. 245, 1039–1049.
Doeller, J.E., Isbell, T.S., Benavides, G., Koenitzer, J., Patel, H., Patel, R.P., Lancaster, J.R., Darley-Usmar, V.M., Kraus, D.W., 2005. Anal. Biochem. 341 (1), 40–51.
Garibay, S.J., Cohen, S.M., 2010. Chem. Commun. 46 (41), 7700–7702.
Guo, J.-H., Kong, D.-M., Shen, H.-X., 2010. Biosens. Bioelectron. 26 (2), 327–332.
Hao, J.N., Yan, B., 2014. J. Mater. Chem. A 2 (42), 18018–18025.
Hao, J.N., Yan, B., 2015. Chem. Commun. 51 (36), 7737–7740.
Hettie, K.S., Klockow, J.L., Glass, T.E., 2014. J. Am. Chem. Soc. 136 (13), 4877–4880.
Jiang, K., Zhang, L., Hu, Q., Yue, D., Zhang, J., Zhang, X., Li, B., Cui, Y., Yang, Y., Qian, G., 2018. Mater. Today Nano 2, 50–57.
Kimura, H., 2011. Exp. Physiol. 96 (9), 833–835.
Li, B., Wen, H.-M., Cui, Y., Zhou, W., Qian, G., Chen, B., 2016. Adv. Mater. 28 (40), 8819–8860.
Li, B., Wen, H.M., Yu, Y., Cui, Y., Zhou, W., Chen, B., Qian, G., 2018. Mater. Today Nano 2, 21–49.
Liu, B., Chen, Y., 2013. Anal. Chem. 85 (22), 11020–11025.
Liu, C., Pan, J., Li, S., Zhao, Y., Wu, L.Y., Berkman, C.E., Whorton, A.R., Xian, M., 2011. Angew. Chem. Int. Ed. 50 (44), 10327–10329.
Liu, T., Zhang, X., Qiao, Q., Zou, C., Feng, L., Cui, J., Xu, Z., 2013. Dyes Pigments 99 (3), 537–542.
Liu, Y., Pan, M., Yang, Q.Y., Fu, L., Li, K., Wei, S.C., Su, C.Y., 2012. Chem. Mater. 24 (10), 1954–1960.
Lu, K., Aung, T., Guo, N., Weichselbaum, R., Lin, W., 2018. Adv. Mater. 30 (37), 1707634.
Luan, Y., Qi, Y., Jin, Z., Peng, X., Gao, H., Wang, G., 2015. RSC Adv. 5 (25), 19273–19278.
Ma, J.X., Huang, X.F., Song, X.Q., Liu, W.S., 2013. Chem. Eur. J. 19 (11), 3590–3595.
Madhuprasad, Bhat, M.P., Jung, H.-Y., Losic, D., Kurkuri, M.D., 2016. Chem. Eur. J. 22 (18), 6148–6178.
Mao, G.-J., Wei, T.-T., Wang, X.-X., Huan, S.-Y., Lu, D.-Q., Zhang, J., Zhang, X.-B., Tan, W., Shen, G.-L., Yu, R.-Q., 2013. Anal. Chem. 85 (16), 7875–7881.
Marambio-Jones, C., Hoek, E.M.V., 2010. J. Nanopart. Res. 12 (5), 1531–1551.
Nagarkar, S.S., Desai, A.V., Ghosh, S.K., 2014. Chem. Commun. 50 (64), 8915–8918.
Nonat, A.M., Harte, A.J., Sénéchal-David, K., Leonard, J.P., Gunnlaugsson, T., 2009. Dalton Trans. 24, 4703–4711.
Pak, Y.L., Li, J., Ko, K.C., Kim, G., Lee, J.Y., Yoon, J., 2016. Anal. Chem. 88 (10), 5476–5481.
Pearson, R.G., 1963. J. Am. Chem. Soc. 85 (22), 3533–3539.
Qian, Y., Karpus, J., Kabil, O., Zhang, S.-Y., Zhu, H.-L., Banerjee, R., Zhao, J., He, C., 2011. Nat. Commun. 2, 495.
Qian, Z., Shan, X., Chai, L., Chen, J., Feng, H., 2014. Chem. Eur. J. 20 (49), 16065–16069.
Rai, M., Yadav, A., Gade, A., 2009. Biotechnol. Adv. 27 (1), 76–83.
Soini, E., Hemmilä, I., 1979. Clin. Chem. 25 (3), 353–361.
Stassen, I., Burtch, N., Talin, A., Falcaro, P., Allendorf, M., Ameloot, R., 2017. Chem. Soc. Rev. 46 (11), 3185–3241.
Szabó, C., 2007. Nat. Rev. Drug Discov. 6 (11), 917–935.
Tan, H., Chen, Y., 2011. Chem. Commun. 47 (45), 12373–12375.
Tangerman, A., 2009. J. Chromatogr. B 877 (28), 3366–3377.
Thomas, S.W., Joly, G.D., Swager, T.M., 2007. Chem. Rev. 107 (4), 1339–1386.
Ubuka, T., 2002. J. Chromatogr. B 781 (1), 227–249.
Wales, D.J., Grand, J., Ting, V.P., Burke, R.D., Edler, K.J., Bowen, C.R., Mintova, S., Burrows, A.D., 2015. Chem. Soc. Rev. 44 (13), 4290–4321.
Wang, J., Ma, Q., Zheng, W., Liu, H., Yin, C., Wang, F., Chen, X., Yuan, Q., Tan, W., 2017. ACS Nano 11 (8), 8185–8191.
Wang, P., Zhang, G., Wondimu, T., Ross, B., Wang, R., 2011. Exp. Physiol. 96 (9), 847–852.
Wang, Z.-Y., Wang, M., Zhang, Y., Zhang, C.-Y., 2018. Chem. Commun. 54 (62), 8602–8605.
Wen, H.-M., Li, L., Lin, R.-B., Li, B., Hu, B., Zhou, W., Hu, J., Chen, B., 2018. J. Mater. Chem. A 6 (16), 6931–6937.
Wen, Y.D., Wang, H., Kho, S.H., Rinkiko, S., Sheng, X., Shen, H.M., Zhu, Y.Z., 2013. PLoS One 8 (2), e53147.
Wu, D., Maurin, G., Yang, Q., Serre, C., Jobic, H., Zhong, C., 2014a. J. Mater. Chem. A 2 (6), 1657–1661.
Wu, P., Zhang, J., Wang, S., Zhu, A., Hou, X., 2014b. Chem. Eur. J. 20 (4), 952–956.
Wu, R., Yao, W.-Z., Chen, Y.-H., Geng, B., Tang, C.-S., 2008. Beijing Da Xue Xue Bao 40 (5), 505–508.
Wu, X., Chen, J., Zhao, J.X., 2013. Analyst 138 (18), 5281–5287.
Xiao, Y., Cui, Y., Zheng, Q., Xiang, S., Qian, G., Chen, B., 2010. Chem. Commun. 46 (30), 5503–5505.
Yang, Q., Jobic, H., Salles, F., Kolokolov, D., Guillerm, V., Serre, C., Maurin, G., 2011a. Chem. Eur. J. 17 (32), 8882–8889.
Yang, Q., Vaesen, S., Ragon, F., Wiersum, A.D., Wu, D., Lago, A., Devic, T., Martineau, C., Taulelle, F., Llewellyn, P.L., 2013. Angew. Chem. 125 (39), 10506–10510.
Yang, Q., Wiersum, A.D., Jobic, H., Guillerm, V., Serre, C., Llewellyn, P.L., Maurin, G., 2011b. J. Phys. Chem. C 115 (28), 13768–13774.

Yang, Y.-Q., He, X.-W., Wang, Y.-Z., Li, W.-Y., Zhang, Y.-K., 2014. Biosens. Bioelectron. 54, 266–272.
Yu, F., Li, P., Song, P., Wang, B., Zhao, J., Han, K., 2012. Chem. Commun. 48 (23), 2852–2854.
Yuan, M., Zhou, W., Liu, X., Zhu, M., Li, J., Yin, X., Zheng, H., Zuo, Z., Ouyang, C., Liu, H., Li, Y., Zhu, D., 2008. J. Org. Chem. 73 (13), 5008–5014.
Zhang, L.-P., Hu, B., Wang, J.-H., 2012. Anal. Chim. Acta 717, 127–133.
Zhang, X., Hu, Q., Xia, T., Zhang, J., Yang, Y., Cui, Y., Chen, B., Qian, G., 2016. ACS Appl. Mater. Interfaces 8 (47), 32259–32265.
Zheng, M., Tan, H., Xie, Z., Zhang, L., Jing, X., Sun, Z., 2013. ACS Appl. Mater. Interfaces 5 (3), 1078–1083.
Zhou, Y., Chen, H.-H., Yan, B., 2014. J. Mater. Chem. A 2 (33), 13691–13697.